GEOMETRIC CHARACTERISTICS ANALYSIS OF ROLLER ENVELOPING END FACE MESH ENGAGEMENT WORM DRIVE

Kai WANG [1*]

In view of the problem of flank clearance of worm gear, roller enveloping end face engagement worm drive is proposed, which adopts the form of inner gearing between double-section worm and worm end face. Based on differential geometry and gear meshing principle, the formulas of meshing equation, spiral curve equation, tooth profile equation and tooth thickness equation are derived. The effect of first boundary function of the transmission pair when the worm gear rotates one turn, change of transmission pair first boundary function with design parameters, the tooth surface undercut curve and spiral lead angle on geometric characteristics of the worm is analyzed. The results show that: the worm gear has five pairs of teeth meshed at the same time, and the tooth profile is very close to a straight line; the variation law of the worm tooth thickness is that the thickness is the thinnest at the engaging teeth pair and thickest at the middle pair; there is no undercut of transmission; the variation law of the spiral lead angle of the roller enveloping end face engagement worm gear tooth is that the angle is the minimum at both ends, and reaches the maximum at the worm throat.

Keywords: worm drive; roller enveloping; end face engagement; geometric characteristic analysis

1. Introduction

The roller enveloping end face engagement worm drive is formed by conjugate engagement of a worm gear with a roller as the tooth and a worm generated by envelope, which can increase the number of meshing teeth and convert the sliding friction between the meshing tooth surfaces into rolling friction, thus improving load carrying capacity, eliminating backhaul errors, reducing wear, lowering losses, increasing efficiency and extending life. This new type of transmission has certain application prospects in the fields of heavy load and precision transmission.

Litvin first proposed the space meshing theory, analyzed various forms of gears, and proposed a general solution method for the relationship between gear tooth surface curvature, which laid a foundation for the study of gear geometry [1]. Tseng [2] studied the principle of spatial meshing, derived the tooth surface

[1] Equipment Manufacturing Institute, Chengdu Vocational & Technical College of Industry, Chengdu, 610218, China. e-mail: 57435843@qq.com

equation. Based on this, a three-dimensional model is established, which lays a foundation for the study of geometrical characteristics of the gear.

Professor Wang Jinge [3] proposed a roller cone enveloping worm drive. A needle bearing can be installed between the roller cone and its journal. The big end of the roller cone can be mounted with an axial rolling bearing, so that the relative sliding between the meshing tooth surfaces is basically converted to relative rolling. Also, the geometric characteristic is analyzed in detail. Chen Yonghong [4] analyzed the influence law of the tooth surface undercutting and gear peak sharpening of plane enveloping drum worm. Liu Zaixin [5] proposed tilted double-roller enveloping worm drive, and analyzed the influence of meshing parameters such as roller radius, roller offset distance and tilt angle on the geometric characteristics of the worm.

In this paper, the geometric characteristics of roller enveloping end face engaging worm drive are studied based on differential geometry and gear meshing principle. The forming principle of roller enveloping end face engagement worm drive is analyzed. The meshing equation of the end face engagement worm is derived and geometric characteristic of the tooth surface is investigated to provide a theoretical basis for further research.

2. Working principle of transmission

The working principle diagram of the roller enveloping end face engagement worm drive is shown in Fig. 1. The worm gear pair is composed of a worm shaft 1, two worms 2, 3, and a worm gear 4. Wherein, the worms 2, 3 are respectively mounted on the left and right sides of the worm shaft 1. The axial position is determined by the step and the shaft sleeve. As a speed reducer, the worm acts as the driving part, the worm gear acts as the driven part, the worm shaft inputs and the worm gear outputs during the working process; the upper tooth surface of the left worm always meshes with the worm gear teeth, and the lower tooth surface of the right worm always meshes with the worm gear teeth. The worms at both ends are in symmetrical engagement with the worm gear, which can eliminate the gap when the worm pair is reversed.

Worm gear teeth of roller enveloping end face engagement worm gear are roller that can rotate around itself, which can convert the sliding friction between the worm gear and the worm meshing tooth surface into rolling friction, thus reducing wear, lowering loss, reducing heat and improving efficiency. For the transmission structure in the paper, a needle bearing is used as the roller. The contact between the gear tooth journal of the worm gear and the inner ring of the needle bearing generates rolling friction. The contact between the outer ring of the needle bearing and the worm tooth surface also generates rolling friction, which

replaces the traditional copper alloy worm gear, reduces the cost and increases the carrying capacity, as shown in Fig. 2.

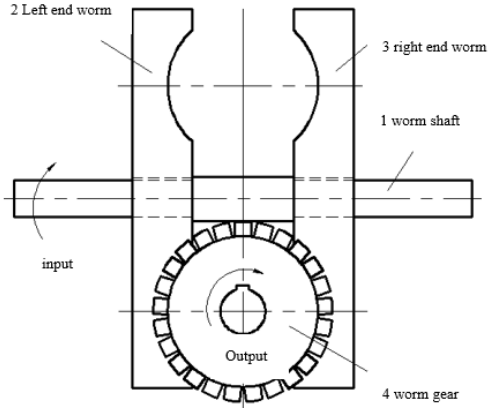

Fig.1. Working principle of roller enveloping end face engagement worm drive

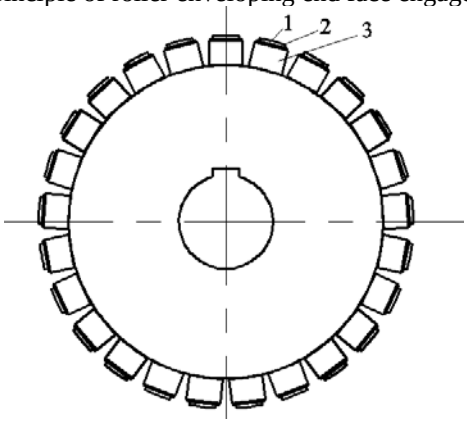

1. worm gear roller 2. jump ring 3. needle bearing

Fig. 2. Worm gear structure

3. Meshing analysis of transmission pair

3.1 Coordinate system setting

According to the differential geometry principle and the forming principle of the roller enveloping end face engagement worm drive, the coordinate system setting is shown in Fig. 3. $\sigma_1\left(i_1, j_1, k_1\right)$ is the worm static coordinate system, $\sigma_2\left(i_2, j_2, k_2\right)$ is the worm gear static coordinate system, $\sigma_{1'}\left(i_{1'}, j_{1'}, k_{1'}\right)$ is the worm active coordinate system, $\sigma_{2'}\left(i_{2'}, j_{2'}, k_{2'}\right)$ is the worm gear active coordinate system, $k_1 = k_{1'}$ is the worm rotating shaft, $k_2 = k_{2'}$ is the worm gear rotating shaft, ω_1 is angular velocity vector of the worm, ω_2 is angular velocity vector of the

worm gear. The worm gear teeth are single rollers, and a coordinate system $\sigma_0(i_0, j_0, k_0)$ is established at the center of the roller column top. The rotation angle of the end face engagement worm around the rotating shaft is φ_1, the rotation angle of the worm gear around the rotating shaft is φ_2, and $\varphi_1/\varphi_2 = \omega_1/\omega_2 = Z_2/Z_1 = i_{12} = 1/i_{21}$. Where, Z_1 is the number of worm head, Z_2 is the number of the worm gear teeth, i_{12} is the transmission ratio; A is the center distance. When $\varphi_1 = \varphi_2 = 0$, the active coordinate system coincides with the static coordinate system. The coordinate of the point O_0 in σ_2 is set as (a_2, b_2, c_2). The moving frame $\sigma_p(e_1, e_2, n)$ is set at the contact point O_p, and the position of the fixed coordinate system S_0 is at the circle center of the roller top.

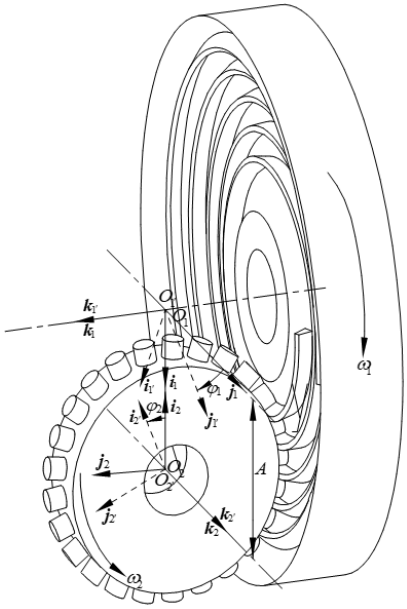

Fig. 3. Coordinate system setting

3.2 Active coordinate system and cylinder equation

The active frame is to establish an orthogonal frame closely related to the surface at each point of the surface, so that each given point on the surface has a unique frame corresponding to it [6]. Fig. 4 is a diagram showing the setting of the active frame of the worm gear roller. It can be seen from the figure that the vector equation of the roller surface in the coordinate system σ_0 is (1):

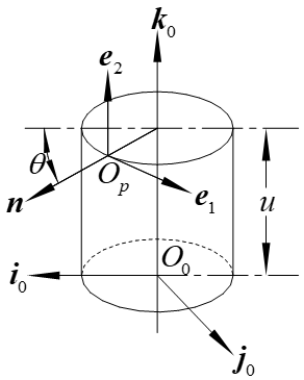

Fig. 4. Active frame setting of the worm gear roller

$$\begin{cases} r_0 = x_0 i_0 + y_0 j_0 + z_0 k_0 \\ x_0 = R\cos\theta \\ y_0 = R\sin\theta \\ Z_0 = u \end{cases} \tag{1}$$

Where, u, θ—cylinder parameters; R—radius of the worm gear roller.

3.3 Meshing function

Based on the principle of gear meshing, the formula for the tooth surface meshing of the worm gear meshing function is:

$$\begin{cases} \Phi = V_n^{(1'2')} = M_1\cos\varphi_2 + M_2\sin\varphi_2 + M_3 \\ M_1 = (a_2 - u)\sin\theta \\ M_2 = 0 \\ M_3 = -i_{21}(\mathrm{a}_2 - u)\cos\theta\ - \mathrm{A}\sin\theta \end{cases} \tag{2}$$

Here, A is the center distance.

4. Geometric characteristic analysis

4.1 Worm tooth surface

The worm tooth surface is enveloping surface formed by the meshing motion of the worm gear with a worm gear tooth meshed therewith as the generatrix. When φ_1 or φ_2 is a constant value, a momentary engagement line can be obtained, and when φ_1 or φ_2 continuously changes, a continuous collection of engagement lines can be obtained. The enveloping surface formed by these

continuous engagement lines is the worm tooth surface [7, 8]. Now, the worm gear surface equation of the worm drive is rewritten as follows:

$$\begin{cases} \mathbf{r}_1 = x_1\mathbf{i}_1 + y_1\mathbf{j}_1 + z_1\mathbf{k}_1 \\ x_1 = -(a_2 - z_0)\cos\varphi_1\cos\varphi_2 - x_0\cos\varphi_1\sin\varphi_2 + y_0\sin\varphi_1 + A\cos\varphi_1 \\ y_1 = -(a_2 - z_0)\sin\varphi_1\cos\varphi_2 - x_0\sin\varphi_1\sin\varphi_2 - y_0\cos\varphi_1 + A\sin\varphi_1 \\ z_1 = (a_2 - z_0)\sin\varphi_2 - x_0\cos\varphi_2 \\ \mathbf{r}_0 = x_0\mathbf{i}_0 + y_0\mathbf{j}_0 + z_0\mathbf{k}_0 \\ u = P_1 / P_2 \\ \varphi_2 = i_{21}\varphi_1 \end{cases} \tag{3}$$

Combining the meshing function with the meshing equation, a functional relationship between generatrix parameters u and θ satisfying the meshing equation is obtained as follows:

$$\begin{cases} \tan\theta = f(u,\varphi_2) = P_3/P_4 \\ P_3 = i_{21}(a_2 - u) \\ P_4 = \cos\varphi_2(a_2 - u) - A \end{cases} \tag{4}$$

The spiral curve equation of the tooth surface of the end face engagement worm is obtained by combining formula (4) and formula (5):

$$\begin{cases} \mathbf{r}_1 = x_1\mathbf{i}_1 + y_1\mathbf{j}_1 + z_1\mathbf{k}_1 \\ x_1 = -(a_2 - z_0)\cos\varphi_1\cos\varphi_2 - x_0\cos\varphi_1\sin\varphi_2 + y_0\sin\varphi_1 + A\cos\varphi_1 \\ y_1 = -(a_2 - z_0)\sin\varphi_1\cos\varphi_2 - x_0\sin\varphi_1\sin\varphi_2 - y_0\cos\varphi_1 + A\sin\varphi_1 \\ z_1 = (a_2 - z_0)\sin\varphi_2 - x_0\cos\varphi_2 \\ \mathbf{r}_0 = x_0\mathbf{i}_0 + y_0\mathbf{j}_0 + z_0\mathbf{k}_0 \\ \tan\theta = f(u,\varphi_2) = P_3/P_4 \\ \varphi_2 = i_{21}\varphi_1 \end{cases} \tag{5}$$

Assuming u is a fixed value and making φ_1 continuously changes, a reducing spiral line on the worm tooth surface can be obtained by equation (5) [7, 8]. When u takes a number of discrete values, a plurality of spiral lines can be obtained, as shown in Fig. 5 and Fig. 6. Fig. 5 shows surface A of spiral line of worm tooth surface on the left and right sides, and Fig. 6 shows surface B of spiral line of worm tooth surface on the left and right sides.

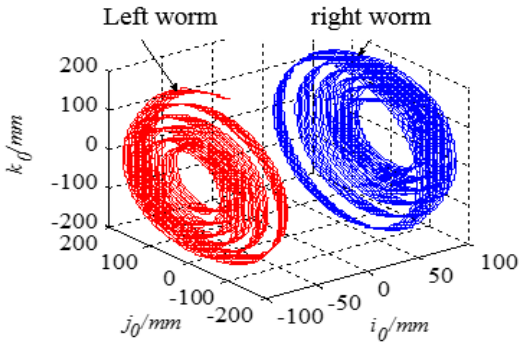

Fig. 5. Worm tooth surface – surface A

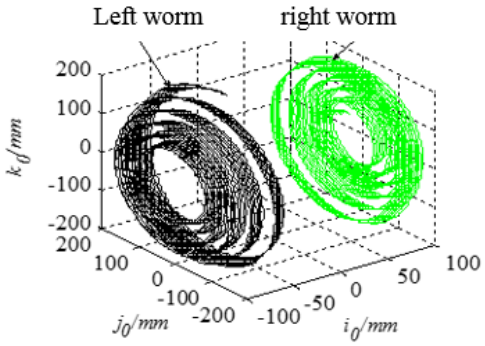

Fig. 6. Worm tooth surface – surface B

4.2 Tooth profile of the worm

Tooth surface section calculation of the end face engagement worm serves an important theoretical basis for studying worm gear peak sharpening and worm tooth thickness detection.

As shown in Fig. 7, the worm is cut by an imaginary plane T, the plane T is parallel to the worm axis, the offset distance is d, and the tooth profile shape of the worm in the axial section T is obtained by the intersection of the plane T and the worm tooth surface. When d is zero, the tooth profile intercepted by the plane T is the symmetrical axial section profile of the worm [7, 9].

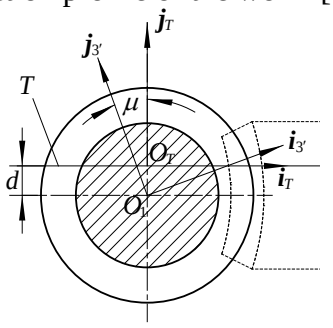

Fig. 7. Worm section

Let the coordinate system $S_T(O_T; \boldsymbol{i}_T, \boldsymbol{j}_T, \boldsymbol{k}_T)$ be fixed to the section planet, and the angle between the bottom vectors $\boldsymbol{i}_{3'}$ and $\boldsymbol{i}_T$ is: $\mu = i/2 (i = 1/i_{21})$, the bottom vector $\boldsymbol{j}_T$ is perpendicular to the plane T. Through the coordinate transformation, the tooth profile equation in the cross section of the worm shaft can be obtained, as shown in equation (6).

$$\begin{cases} \mathbf{r}_1 = x_1\mathbf{i}_1 + y_1\mathbf{j}_1 + z_1\mathbf{k}_1 \\ x_1 = -(a_2 - z_0)\cos\varphi_1\cos\varphi_2 - x_0\cos\varphi_1\sin\varphi_2 + y_0\sin\varphi_1 + A\cos\varphi_1 \\ y_1 = -(a_2 - z_0)\sin\varphi_1\cos\varphi_2 - x_0\sin\varphi_1\sin\varphi_2 - y_0\cos\varphi_1 + A\sin\varphi_1 \\ z_1 = (a_2 - z_0)\sin\varphi_2 - x_0\cos\varphi_2 \\ \boldsymbol{r}_0 = x_0\boldsymbol{i}_0 + y_0\boldsymbol{j}_0 + z_0\boldsymbol{k}_0 \\ \tan\theta = f(u,\varphi_2) = P_3/P_4 \\ \varphi_2 = i_{21}\varphi_1 \\ x_T = x_1\cos\mu - y_1\sin\mu \\ y_T = x_1\sin\mu + y_1\cos\mu - d \\ z_T = z_1 \\ y_T = 0 \end{cases} \tag{6}$$

If the value u and φ are determined in the tooth profile equation, then a point on the section profile can be obtained. A series of continuous values φ can be used to obtain a series of points on the tooth profile of the axial section. These points can be smoothly connected to obtain the axial tooth curve of the worm [3]. Due to the space length limitation, d=0, and the left worm axial section tooth profile shape of the roller enveloping end face engagement worm drive with center distance A=125mm, transmission ratio i=25 is shown in Fig. 8.

Fig. 9 is worm axial section profile shape of surfaces 1, 2 of the tooth profile A calculated by the tooth profile equation.

(1) Tooth profile A

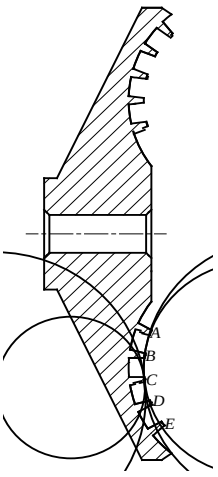

Fig. 8. Worm axial section tooth profile

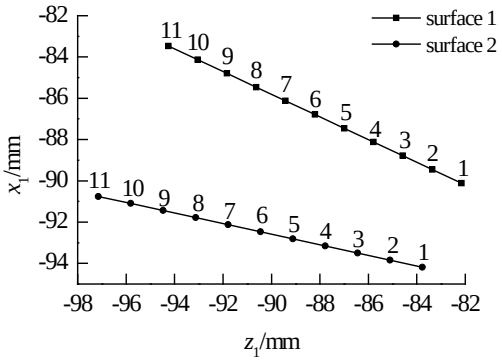

Fig. 9. Axial section tooth profile A

4.3 Calculation of worm axial tooth thickness

From the design point of view, the worm strength design has a certain relationship with the worm tooth thickness; from the perspective of detection, for non-modular worm, tooth thickness detection during the detection process is an important part in determination of coincidence of the theoretical model and the

prototype sample. In order to ensure the strength design and manufacturing precision of the worm, it is necessary to calculate the tooth thickness.

As shown in Fig. 10, R_{12} indicates the section radius of the roller enveloping end face inner engagement worm drive in the worm gear height direction, S_i indicates the chordal tooth thickness.

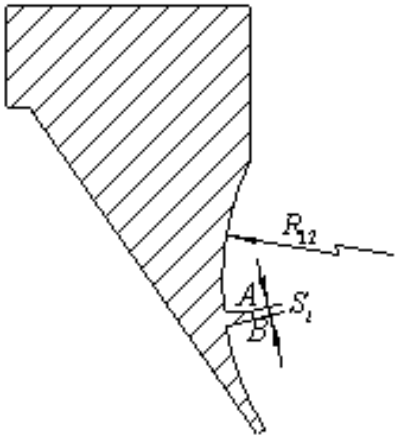

Fig. 10. Tooth thickness on any circle

Through the formulas (7) and (8), the tooth thickness calculation process is as follows:

$$\begin{cases} r_1 = x_1 i_1 + y_1 j_1 + z_1 k_1 \\ x_1 = -(a_2 - z_0)\cos\varphi_1\cos\varphi_2 - x_0\cos\varphi_1\sin\varphi_2 + y_0\sin\varphi_1 + A\cos\varphi_1 \\ y_1 = -(a_2 - z_0)\sin\varphi_1\cos\varphi_2 - x_0\sin\varphi_1\sin\varphi_2 - y_0\cos\varphi_1 + A\sin\varphi_1 \\ z_1 = (a_2 - z_0)\sin\varphi_2 - x_0\cos\varphi_2 \\ \boldsymbol{r}_0 = x_0\boldsymbol{i}_0 + y_0\boldsymbol{j}_0 + z_0\boldsymbol{k}_0 \\ \tan\theta = f(u,\varphi_2) = P_3/P_4 \\ \varphi_2 = i_{21}\varphi_1 \\ x_T = x_1\cos\mu - y_1\sin\mu \\ y_T = x_1\sin\mu + y_1\cos\mu - d \\ z_T = z_1 \\ y_T = 0 \\ (A - x_T)^2 + z_T^2 = R_{12}^2 \end{cases} \tag{7}$$

In the calculation, by presetting values u and d, and determining the value R_{12} in the section, solve equation (8) and then the coordinate value $A(A_{x1T}, A_{z1T})$ and $B(B_{x1T}, B_{z1T})$ of point A and B can be obtained, so that the chordal tooth thickness S_i can be obtained:

$$S_i = \sqrt{(A_{x1T} - B_{x1T})^2 + (A_{z1T} - B_{z1T})^2} \tag{8}$$

4.4 Undercut curve of the worm tooth surface

In order to avoid undercut, first boundary curve is required to be smaller than the root diameter of the worm. The first boundary function of the drive is:

$$\Psi = \Phi_t + \omega_2^{(12)} v_1^{(12)} - \omega_1^{(12)} v_2^{(12)} - (v_1^{(12)})^2 / R \tag{9}$$

When A=125mm, Z_1=1, Z_2=25, k_1=0.3, R=11mm, the value of the first boundary function of the transmission pair when the worm gear rotates one turn is shown in Fig. 11, here, k_1 is Laryngeal coefficient of the worm. It can be seen from the figure that the first boundary function of the transmission pair is first reduced and then increased as the worm gear rotates, which reaches the maximum at the beginning and end of engagement, but still less than zero. The variation trend of the first boundary function with the design parameters at the starting position of the worm gear rotation is shown in Fig. 12. The first boundary function increases with the increase of the roller radius, and decreases with the increase of worm gear angle, throat radius coefficient, center distance and the number of worm gear teeth. To avoid undercut of the transmission pair, the roller radius should not be too large, while the throat radius coefficient, the center distance and the number of worm gear teeth should not be too small.

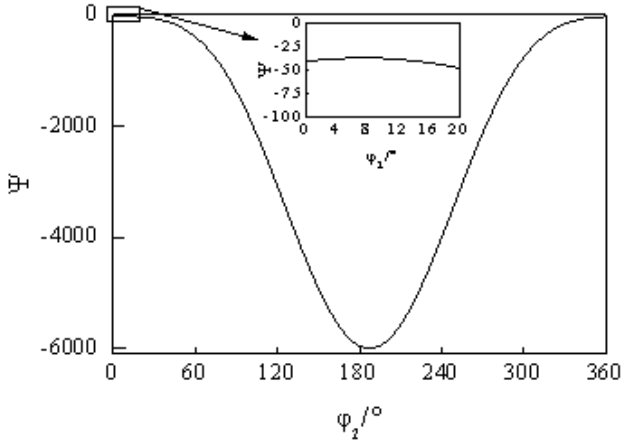

Fig. 11. First boundary function when the worm gear rotates one turn

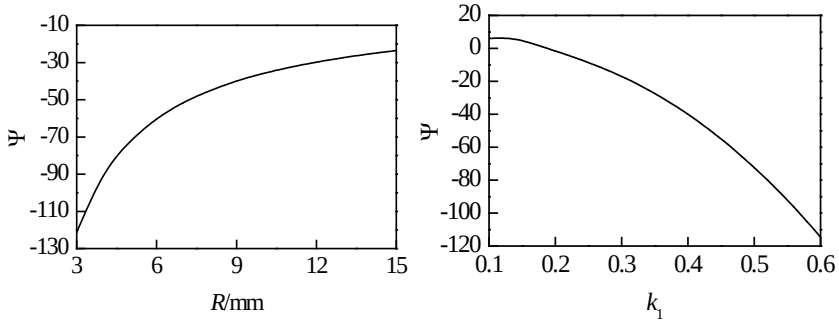

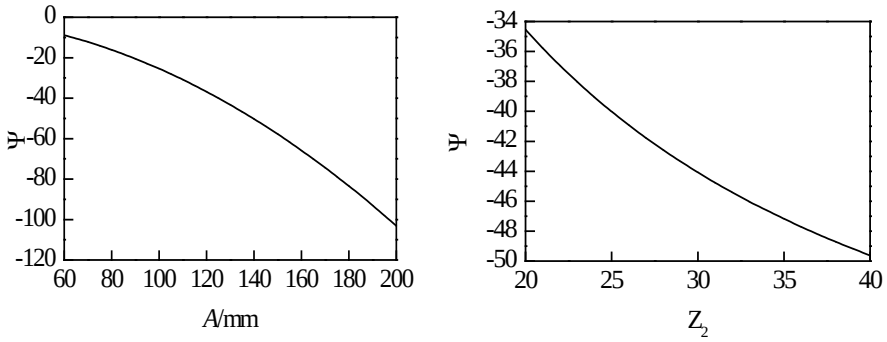

Fig. 12. Variation of transmission pair first boundary function with design parameters

The first boundary condition according to the gear space meshing principle [10, 11] is as follows:

$$\begin{cases} \Phi = 0 \\ \Psi = 0 \end{cases} \tag{10}$$

First boundary curve is a spiral line that is closer to the worm axis but away from the worm root diameter.

In order to intuitively determine the undercut condition of the roller enveloping end face engagement worm drive, the method of determining the two-dimensional undercut line: is to project the coordinates (x_1, y_1, z_1) of the first boundary curve on the plane $R_w - z_1$, as follows:

$$\begin{cases} R_w = \sqrt{x_1^2 + y_1^2} \\ z_1 = z_1 \end{cases} \tag{11}$$

Fig. 13 is a two-dimensional undercut judgment line of the tooth surface of the roller enveloping end face engagement worm drive. It can be seen from the figure that the undercut judgment curve does not coincide with or exceed the arc radius of the worm tooth root, so it can be determined that there is no undercut phenomenon in the transmission.

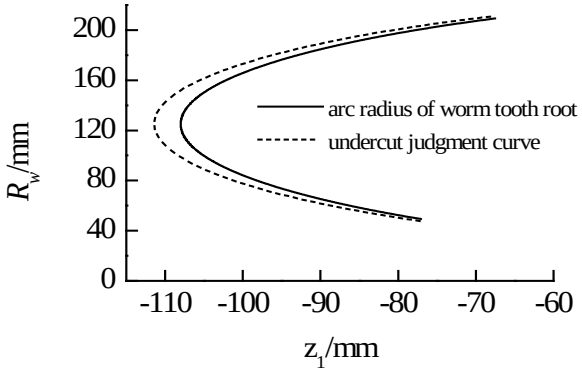

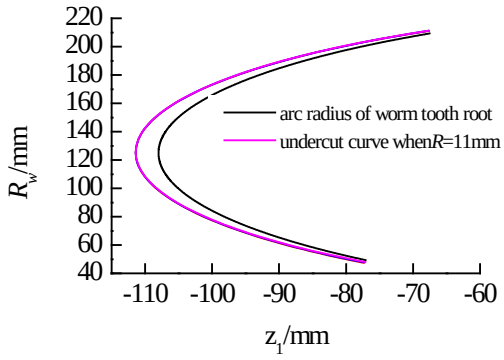

Fig. 13. Undercut curve on the worm tooth surface

4.5 Worm spiral lead angle

The acute angle λ between the tangent $\boldsymbol{n}_p$ of any point on the spiral line and radial section passing point P is the spiral lead angle [7, 10, 11] of the worm tooth surface at that point, which A and B are the two points on the radial section, as shown in Fig. 14.

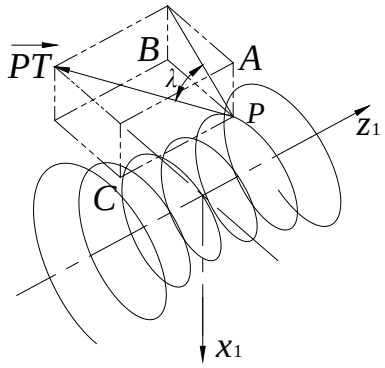

Fig. 14. Worm spiral lead angle

According to differential geometry and the principle of spatial meshing, it can be known that the tangent of the intersection of the two curved surfaces is perpendicular to normal of the two intersect surfaces at the normal vector of point P, $\boldsymbol{n}_b$ is normal vector of rotating surface at point P. Then the tangent $\boldsymbol{n}_p$ of the worm spiral line at point P is [3, 7, 11]:

$$\boldsymbol{n}_p = n_a \times n_b \tag{12}$$

In the roller enveloping end face engagement worm drive, the contact line is distributed on the enveloping generatrix, so the normal vector of the contact line is consistent with the enveloping generatrix [12, 13]. Write it in $O_{1'}(i_{1'}, j_{1'}, k_{1'})$, then:

$$\begin{cases} \boldsymbol{n}_a = n_{ax}\boldsymbol{i}_{1'} + n_{ay}\boldsymbol{j}_{1'} + n_{az}\boldsymbol{k}_{1'} \\ n_{ax} = \cos\theta\sin\varphi_1 + \sin\theta\cos\varphi_1\sin\varphi_2 \\ n_{ay} = \cos\theta\cos\varphi_1 - \sin\theta\sin\varphi_1\sin\varphi_2 \\ n_{az} = -\sin\theta\cos\varphi_2 \end{cases} \tag{13}$$

Through mathematical derivative transformation, it can be obtained that:

$$\begin{cases} \boldsymbol{n}_b = n_{bx}\boldsymbol{i}_{1'} + n_{by}\boldsymbol{j}_{1'} + n_{bz}\boldsymbol{k}_{1'} \\ n_{bx} = x_1 / (1 - A / \sqrt{x_1^2 + y_1^2}) \\ n_{by} = y_1 / (1 - A / \sqrt{x_1^2 + y_1^2}) \\ n_{bz} = z_1 \end{cases} \tag{14}$$

Here, A is the center distance.

Substitute (13), (14) into equation (12), then tangent vector $\boldsymbol{n}_p$ of the worm spiral line at point P is:

$$\begin{cases} \boldsymbol{n}_p = A_1\boldsymbol{i}_{1'} + B_1\boldsymbol{j}_{1'} + C_1\boldsymbol{k}_{1'} \\ A_1 = n_{ay}n_{bz} - n_{az}n_{by} \\ B_1 = n_{az}n_{bx} - n_{ax}n_{bz} \\ C_1 = n_{ax}n_{by} - n_{ay}n_{bx} \end{cases} \tag{15}$$

Then the formula of the spiral lead angle is:

$$\lambda = \arccos\frac{\sqrt{A_1^2 + B_1^2}}{\sqrt{A_1^2 + B_1^2 + C_1^2}} \tag{16}$$

Figs. 15 to 19 show variation curves of the spiral lead angles of A and B surfaces on the left and right sides of the root circle, reference circle and tip circle of the roller enveloping end face engagement worm drive.

According to the analysis, the spiral lead angle of the left and right sides of the left worms is equal when the roller enveloping end face engagement worm drive is at z1=94.0308. When z1=-94.0308, the spiral lead angle of A and B surfaces of the right worm is also equal.

For the left and right worms, the spiral lead angle curve is symmetrically distributed, and the upper tooth surface of the left worm is symmetrical with the lower tooth surface of the right worm. That is, surface A of the left worm is symmetrical with surface B of the right worm. The maximum value 1.6155° is reached when z1=83.8438mm and z1=-83.8438mm. The lower tooth surface of the left worm is symmetrical with the upper tooth surface of the right worm. That is, surface B side of the left worm is symmetrical with surface A of the right worm. The maximum value 1.6155° is achieved when z1=74.2144 mm and z1=-74.2144 mm.

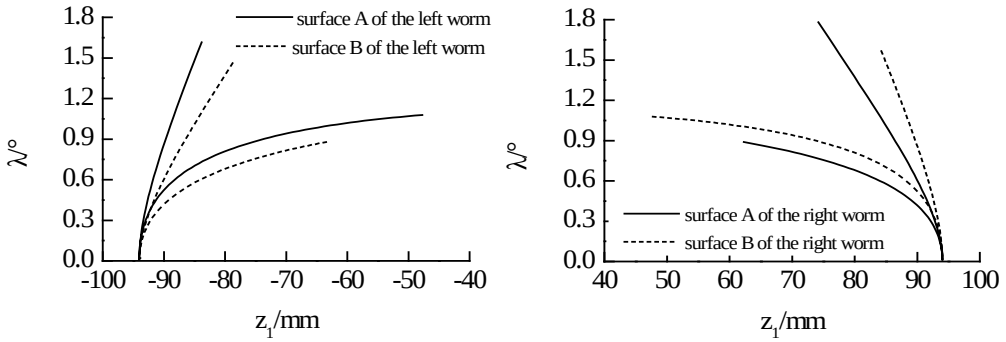

Fig. 15. Spiral lead angle of end face worm root circle

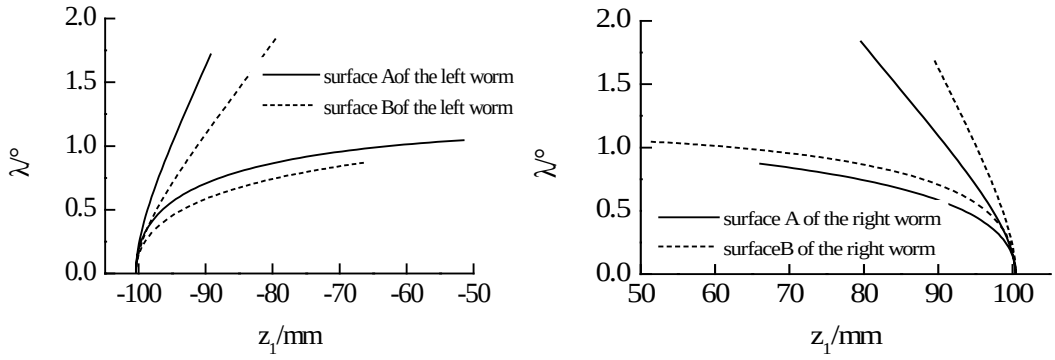

Fig. 16. Spiral lead angle of end face worm reference circle

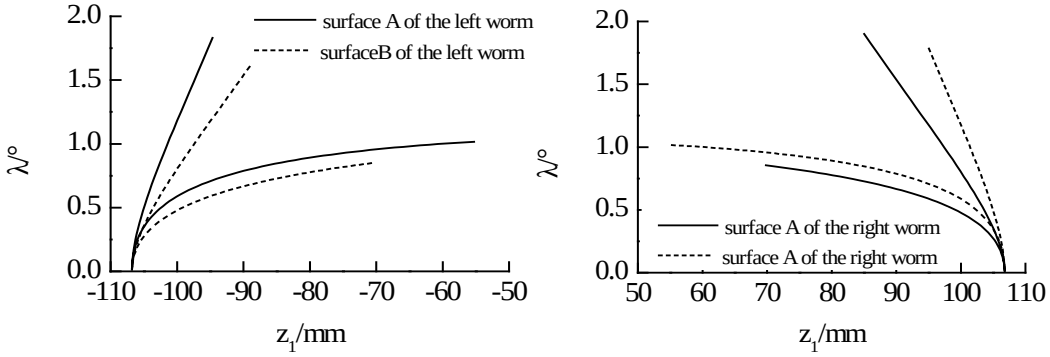

Fig. 17. Spiral lead angle of end face worm tip circle

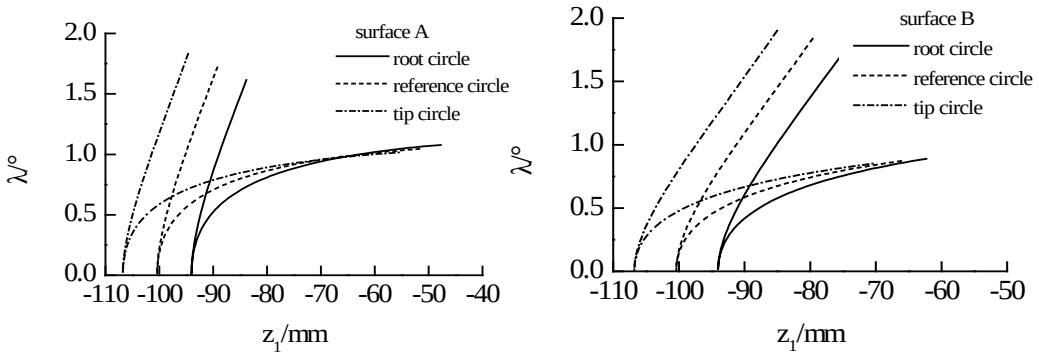

Fig 18. Spiral lead angle of left worm

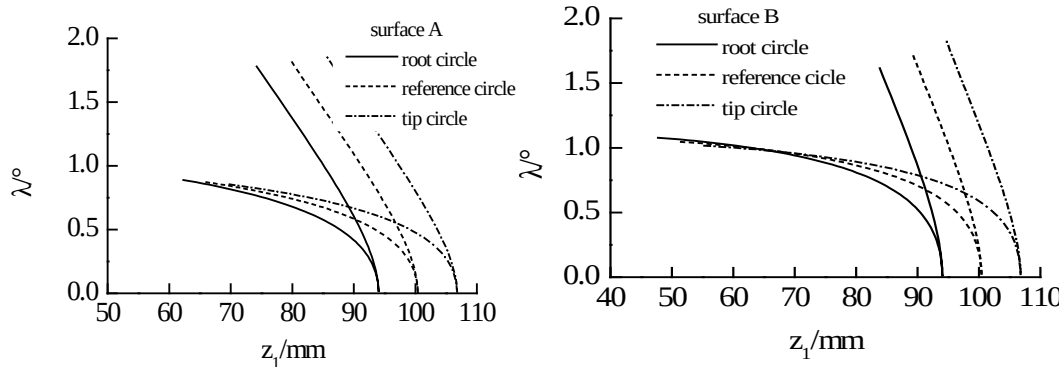

Fig 19. Spiral lead angle of right worm

5. Conclusion

In this paper, transmission pair of roller enveloping end face engagement worm gear is taken as the research object. The transmission working principle and meshing performance are discussed. The geometric characteristics of the worm pair are analyzed. The following conclusions are obtained:

1) The worm drive has five pairs of teeth meshed at the same time, and the tooth profile is very close to a straight line.

2) The variation law of the worm tooth thickness is that the thickness is the thinnest at the engaging teeth pair and thickest at the middle pair.

3) The undercut law is studied, and it is determined that there is no undercut in the transmission.

4) The variation law of the spiral lead angle of the tooth surface of the roller enveloping end face gear worm is that the angle reaches the minimum at both ends and reaches the maximum at the worm throat.

5) This kind of worm does not undercut, with good processing performance.

REFERENCES

[1]. *F. L. Litvin, I. Gonzalez-Perez, K. Yukishima, A. Fuentes, K. Hayasaka*, "Design, simulation of meshing, and contact stresses for an improved worm gear drive", Mechanism & Machine Theory, **vol. 42**, no. 8, 2007, pp. 940-959.

[2] *R. T. Tseng, C. B. Tsay*, "Mathematical model and surface deviation of cylindrical gears with curvilinear shaped teeth cut by a hob cutter", ASME Journal of Mechanical Design, **vol. 45**, 2005, pp. 982–987.

[3]. *J. Wang*, "Rolling cone enveloping hourglass worm gearing", Chengdu: Sichuan Publication House of Science and Technology, 2000, pp. 10-65.

[4]. *Y. Chen*, "Theoretical and Experimental Investigations on Planar Tooth Internal Gear Enveloping Crown Worm Drive", Chongqing: Chongqing University, 2013.

[5]. *Z. Liu, J. Wang, J. Zhang*, "Geometrical Characteristics Analysis of Non-Parallel Double-Roller Enveloping Hourglass Worm Gearing", Transactions of Beijing Institute of Technology, **vol. 33**, no. 5, 2013.

[6]. *B.A. Lopatin, S.V. Plotnikova, S.A. Khaustov*, "Involute Helical-bevel Gearing", Procedia Engineering, **vol. 129**, 2015, pp. 891-895.

[7]. *Z. Liu*, "Research on the Inclined Double-roller Enveloping Hourglass Worm Gears", Chengdu: Sichuan University, 2014.

[8]. *X. Deng, J. Wang, J. Zhang, et al.* "Theoretical study on real tooth surface of non-backlash double-roller enveloping hourglass worm", Journal of South-west Jiaotong University, **vol. 45**, no. 2, 2010, pp. 222-226.

[9]. *L. Hong*, "Study on the Anti-backlash Double-roller Enveloping Hourglass Worm Gearing", Chengdu: Xihua University, 2007.

[10]. *S. Wang*, "Concise tutorial on gear meshing theory", Tianjin: Tianjin University Press, 2005.

[11]. *X. Wu*, "Principle of gearing", Xi'an: Xi'an Jiaotong University Press, 2009, pp. 120-240.

[12]. *Y. Zhao, C. Huai, Y. Zhang*, "Compound Modification of Globoidal Worm Drive with Variable Parameters", Applied Mathematical Modelling, 2017.

[13]. *H. Lu, Z. Liu, S. Wang*, "Digitization modeling and CNC machining for enveloping surface parts", The International Journal of Advanced Manufacturing Technology, **vol. 73**, no. 1-4, 2014, pp. 209-227.